RSC Advances

PAPER

View Article Online
View Journal | View Issue

Published on 07 July 2016. Downloaded by Indian Institute of Technology Mandi on 6/18/2020 12:12:14 PM.

Cite this: *RSC Adv.*, 2016, **6**, 67143

Design, development, EUVL applications and nano mechanical properties of a new HfO_2 based hybrid non-chemically amplified resist†

Pulikanti Guruprasad Reddy,[a] Narsimha Mamidi,[a] Pawan Kumar,[b] Satinder K. Sharma,*[b] Subrata Ghosh,[a] Kenneth E. Gonsalves*[a] and Chullikkattil P. Pradeep*[a]

Received 24th April 2016
Accepted 7th July 2016

DOI: 10.1039/c6ra10575k

www.rsc.org/advances

A new HfO_2 based hybrid polymer HfO_2–methacrylate–MAPDST (HMM, M_w ∼27 885 g mol^{-1}) was synthesized by reacting the hybrid monomer HfO_2–methacrylate (HM) with (methacryloyloxy)phenyldimethylsulfoniumtriflate (MAPDST) in the presence of azobisisobutyronitrile (AIBN) as a radical initiator in tetrahydrofuran and acetonitrile (2 : 1; v/v) at 60 °C for Extreme Ultraviolet Lithography (EUVL) applications as a non-chemically amplified resist (n-CAR) material. Transmission Electron Microscope (TEM) and Dynamic Light Scattering (DLS) analyses revealed the particle sizes of HM and HMM hybrids as ∼3–5 nm and ∼12 nm respectively. Thin films of thickness ∼53 nm were prepared by spin coating 3% (w/v) solutions of HMM in methanol onto 4″ p-type Si wafers consisting of a 40 nm hexamethyldisilazane (HMDS) under layer. The films were then subjected to EUV exposure at a dose of 51.7127 mJ cm^{-2} on a micro exposure tool (MET) with an Advanced Light Source (ALS) at SEMATECH Berkeley using standard mask IMO228775 with field R4C3 (LBNL low flare bright-field). The EUV E_0 dose used for the exposure was 22 mJ cm^{-2}. Field Emission Scanning Electron Microscope (FE-SEM) micrographs of the EUV exposed hybrid resist films showed isolated line patterns of 80, 70, 60, 50, 45, 40, 35 and 30 nm for 5 : 1 duty cycle, of which 80 to 50 nm line patterns were well resolved, whereas patterns of 45 to 30 nm or higher resolutions exhibited undesirable traits like bridging, fracturing, de-adhesion, peel-off and pattern collapse. To comprehend the reasons behind these undesirable traits, nano-mechanical properties (modulus and adhesion) of the EUV exposed and developed resist patterns were investigated by using Peak Force-Quantitative Nano-Mechanical (PF-QNM) tapping mode Atomic Force Microscope (AFM). These studies revealed ∼18% and ∼19% reductions in Derjaguin–Müller–Toporov (DMT) modulus and adhesion magnitudes respectively with an increase in isolated line pattern resolution from 80 to 30 nm for 5 : 1 duty cycles. The reduction in modulus and adhesion magnitudes might have caused the observed fracturing, peel-off and collapse of the high resolution line patterns during the pattern development processes.

Introduction

Extreme ultra-violet lithography (EUVL) is perceived as one of the next generation technologies for fabricating microelectronic devices of 20 nm technology nodes and beyond.[1,2] However, there are many roadblocks still to overcome before commercializing this technique for sub 20 nm applications. For sub-20 nm patterning, use of thinner resist films is preferred in order to prevent pattern collapse from high aspect ratios. An aspect ratio of 2 : 1 under such conditions requires resist films of thickness ∼30–40 nm. However, thin resist films based on neat organic polymers face extremely challenging hurdles such as poor photon absorption, moderate etch resistance and limited gains for sub-20 nm high resolution patterning.[3,4] This poses the serious challenge of developing highly sensitive and etch resistant photoresists capable of forming thinner films to prevent pattern collapse and at the same time allow efficient pattern transfer for high resolution lithographic applications.

In recent years, organic/inorganic hybrid photoresists have received significant attention due to their combined functionalities arising from both inorganic and organic components. It has been shown that the incorporation of inorganic units like metal nanoparticles endow the organic photoresists with high etch resistance while maintaining the required processing properties of soft materials.[5,6] Problems such as pattern collapse and poor pattern transfer in sub-30 nm region suffered by

[a]*School of Basic Sciences, Indian Institute of Technology Mandi, Kamand-175 005, Himachal Pradesh, India. E-mail: pradeep@iitmandi.ac.in; kenneth@iitmandi.ac.in; Fax: +91 1905 267 009; Tel: +91 1905 267 045*

[b]*School of Computing and Electrical Engineering, Indian Institute of Technology Mandi, Kamand-175 005, Himachal Pradesh, India. E-mail: satinder@iitmandi.ac.in*

† Electronic supplementary information (ESI) available: Characterization data of hybrids. See DOI: 10.1039/c6ra10575k

This journal is © The Royal Society of Chemistry 2016

Published on 07 July 2016. Downloaded by Indian Institute of Technology Mandi on 6/18/2020 12:12:14 PM.

conventional organic polymer-based photoresists could also be reduced by using hybrid resists. Polyhedral oligomeric silsesquioxane (POSS), molecular organometallics, metal oxide nanoparticles *etc.* are examples of inorganic components used in photoresist formulations.[7–14] Particularly, metal oxide nanoparticles have received considerable attention as inorganic components for next generation hybrid photoresists.[15,16] One significant advantage of metal oxide nanoparticles based photoresists is their re-inforced mechanical strength and accompanying high etch resistance compared to that of neat organic polymer based resists.[7–16] Advantages of metal oxides based resists also include their higher optical densities, which enable them to harvest EUV photons efficiently to provide superior lithographic performances including enhanced sensitivity and lower shot noise.[17] The metal oxides are known to absorb EUV photons with optical densities that are higher than that of carbon.[11] Oxide nanoparticle EUV (ONE) negative resists for 22 nm patterns with high sensitivity was reported by Ober *et al.* in 2011.[18] Further studies on zirconia or hafnia nanoparticle based hybrid resists have also demonstrated the applicability of ONE resists for high resolution patterning (~20 nm line-spaces).[5] Often, photo acid generators (PAG) were part of such chemically amplified resist (CAR) formulations, which may lead to pattern roughness at high resolutions.[19] In this respect, non-chemically amplified resists (n-CARs), which show low Line Edge Roughness (LER) and Line Width Roughness (LWR), are projected superior to CARs for sub-20 nm patterning applications.[20,21] In n-CARs, materials that are directly sensitive to radiations are used without utilising the concept of chemical amplification. However, the development of n-CARs often lags behind that of CARs mainly due to their low sensitivity.[20] Therefore, incorporation of inorganic components (such as HfO_2 nanoparticles) is envisaged to improve the sensitivity of n-CARs by enhancing their EUV absorption.

Furthermore, during the resist development processes, especially for sub-20 nm pattering applications, pattern collapse is more likely to occur due to the dominant capillary forces causing fracturing, bending, line folding, delamination or peel-off and de-adhesion of patterns from the substrate.[22,23] Therefore, measurement of nano-mechanical properties like Derjaguin–Müller–Toporov (DMT) modulus and adhesion may lead to a better understanding of the mechanisms that lead to pattern collapse and hence would ultimately help in designing improved resists. However, such nano-mechanical properties are not easy to evaluate, especially at higher resolutions. A few research attempts have already been reported in this direction,[24,25] however a direct, non-destructive nano-mechanical technique for the determination of DMT modulus and adhesion for n-CAR line pattern analysis has not yet been reported.

Considering the above, herein we report the design and development of a new hybrid n-CAR based on organic monomer (methacryloyloxy)phenyldimethylsulfoniumtriflate (MAPDST)[21] and HfO_2–methacrylate (HM) hybrid monomer. In MAPDST based photoresists, photon directed polarity changes occur at the sulfonium centers causing solubility difference to the exposed and un-exposed regions leading to pattern transfer.[17,21,26] It was expected that a combination of MAPDST and HfO_2 nanoparticles may lead to combined functionalities of both the components leading to an improved resist formulation for EUVL applications. The nano-mechanical properties of the EUV line-patterns were evaluated by using non-destructive Atomic Force Microscope (AFM) technique Peak Force-Quantitative Nano-Mechanical (PF-QNM) analyses. It is expected that a detailed analysis of line modulus, adhesion and topography of the patterns leading to a clear understanding of such fundamental nano-mechanical properties may help in designing improved EUV resist formulation for next generation lithography applications.

Experimental section

Chemicals and reagents

Hafnium(IV) *tert*-butoxide, acetic acid and diethylether were purchased from Sigma-Aldrich and used as received. Methacrylic acid (MA) and tetramethylammonium hydroxide (TMAH) were purchased from Acros Organics. Tetrahydrofuran (THF) was dried using sodium wire/benzophenone and acetonitrile (CH_3CN) was dried using calcium hydride (CaH_2). AIBN (azobisisobutyronitrile) was purchased from Paras Polymers, India and recrystallized twice before use in polymerizations. HfO_2–acetate (HA) and HfO_2–methacrylate (HM) were synthesized according to reported procedures.[14,27] MAPDST monomer was synthesized by following a reported procedure.[21]

FT-IR, NMR, TGA, EDX and DLS analyses

FT-IR spectra were recorded in 4000–400 cm^{-1} range using a Perkin-Elmer Spectrum-2 spectrophotometer at a resolution of 4 cm^{-1} averaging 16 scans per spectrum. ^1H, ^{13}C and ^{19}F NMR were recorded on Jeol JNM ECX 500 MHz spectrometer using DMSO-d_6/$CDCl_3$ as solvents. Thermogravimetric analyses (TGA) were performed on NETZSCH STA 449 F1 JUPITER Series instrument. The heating rate employed was 10 °C min^{-1} under N_2 atmosphere over a temperature range of 25–800 °C. Energy-dispersive X-ray spectroscopy (EDX) analyses of HMM hybrid polymer were conducted on FEI-Nova nano SEM-450. Dynamic light scattering studies (DLS) were conducted on a Malvern, Zetasizer instrument.

TEM and GPC analyses

The microstructure and morphology analyses of HA, HM and HMM hybrids were performed by using High Resolution-Transmission Electron Microscope (HR-TEM), JEOL-JEM-200FS, operated at 200 keV with a 1.9 Å point-to-point resolution. For HR-TEM studies, the samples were first suspended in ethanol to disperse the powders followed by deposition of a drop of the suspension on lacey carbon copper grid used as a TEM support.

Molecular weight and polydispersity index (PDI) of HMM were determined by performing gel permeation chromatography (GPC) analyses using PL gel mixed C 10 μm column on a 1260 Infinity Series instrument from Agilent. DMF with 1% LiBr was used as mobile phase at a flow rate of 1 mL min^{-1} and a column temperature of 70 °C.

 This journal is © The Royal Society of Chemistry 2016

Published on 07 July 2016. Downloaded by Indian Institute of Technology Mandi on 6/18/2020 12:12:14 PM.

Synthesis of HMM hybrid polymer

HM (0.100 g, 20%), MAPDST monomer (0.400 g, 80%) and AIBN (1 wt% relative to the combined weight of the monomers) were dissolved in a mixture of THF–CH_3CN (2 : 1, v/v) in a vial with a side arm under N_2 atmosphere and the resulting solution was siphoned-off to the polymerization flask equipped with a silicone septum and a Teflon coated stirring bar. The mixture, after 1 h of N_2 purging, was left under magnetic stirring at 60 °C for 48 h under N_2 atmosphere. After completion of the reaction, the mixture was poured slowly into diethyl ether (300 mL) and the separated solid was washed with acetonitrile. The resulting crude product was dissolved in methanol and then re-precipitated using diethyl ether. The separated white solid was filtered off and dried in a temperature-controlled hot-air oven at 50 °C for 24 h. Yield: 0.230 g (52%). FT-IR: ν_{max}/cm^{-1} 3027–2935 (CH), 1755 (C=O), 1588 (C=O asymmetric), 1500 (C=O symmetric), 1421 (C=C), 1254 (CF_3), 1160, 1086, 1023, 1000, 877, 836, 814, 637–560–501–428 (HfO_2). ^{1}H NMR (500 MHz, DMSO-d_6) δ_H 8.12 (2H, br. s, ArH), 7.44 (2H, br. s, ArH), 3.21 (6H, s, $S(CH_3)_2$), 2.38–2.00 (4H, br. peak, CH_2 polymeric), 1.5–1.11 (6H, br. peak, CH_3 aliphatic); ^{13}C NMR (125 MHz, DMSO-d_6) δ_C 174.59 (C=O), 162.48 (O–C=O), 153.86, 132.32, 131.78, 123.99, 123.31, 117.39 (aromatic, CF_3), 45.49 (CH_2), 29.00 (SCH_3), 28.54, 25.26, 22.64, 21.87, 19.01 (CH_3 aliphatic). ^{19}F NMR (376 MHz; DMSO-d_6) δ_F −77.64 (3F, s, CF_3).

Thin film formation

Thin films of HMM having a thickness of ~53 nm were prepared by spin coating its 3% (w/v) solution in methanol at 5000 rpm for 60 s onto 4″ p-type Si wafers consisting of 40 nm hexamethyldisilazane (HMDS) under layer. The films thus obtained were subjected to post apply bake (PAB) and post exposure bake (PEB) at 90 °C for 120 s and 100 °C for 90 s respectively. The EUV exposed patterns were developed in 200 μL TMAH stock solution in 50 mL DI water for 180 s followed by rinsing with DI water for 5 s.

EUV exposure and FE-SEM characterization

EUV exposure of the spin coated HMM hybrid n-CAR films on HMDS wafers were performed on a micro exposure tool (MET) at the Advanced Light Source (ALS) in SEMATECH Berkeley. All the exposures were performed by using ALS MET Standard Mask IMO228775 with field R4C3 (LBNL low flare bright-field). The EUV E_0 dose used for the exposure was 22 mJ cm^{-2}. The critical dimension (CD) analysis were accomplished using a Carl Zeiss Ultra Plus Field Emission Scanning Electron Microscope (FE-SEM). The thickness of isolated line patterns was measured by using AFM line profile measurements and found to be ~52.75 ± 0.1 nm indicating a similar thickness as found for original resist film (see ESI, Fig. S1†).

Nano-mechanical property analyses

The surface morphology as well as the materials properties required for nano-mechanical analyses were obtained by using Atomic Force Microscope (AFM) (Dimension Icon, Bruker) operating in Peak Force tapping mode. The standard tapping cantilever (TESPA) from Bruker with a nominal tip radius of 8 nm was used for both imaging and Peak Force-Quantitative Nano-Mechanical (PF-QNM) measurements. Aluminium coated probes having a resonant frequency of ~325 kHz, spring constant of 42 N m^{-1} and tip half angle of 18° were used in these experiments. By calibrating the deflection sensitivity, cantilever spring constant and tip radius, the force-distance characteristics were derived yielding quantitative information about elastic modulus, adhesion, dissipation energy and deformation properties of the line patterns.

Results and discussion

Synthesis and characterization

The HMM hybrid polymer photoresist was synthesized in a three step process as shown in Scheme 1. Firstly, HfO_2–acetate (HA) was synthesized as a fine white powder by the hydrolysis and condensation of hafnium(IV) *tert*-butoxide in presence of acetic acid at 60 °C for 2 days.[14,27] Secondly, the hybrid monomer HfO_2–methacrylate (HM) was synthesized as a light brown solid by ligand exchange of HA with methacrylic acid in propylene glycol monomethyl ether acetate (PGMEA) solvent[27] (see ESI† for HA and HM synthesis). Finally, the HMM hybrid polymer was synthesized by the co-polymerization of HM and MAPDST monomers in 20 : 80 weight ratio in presence of AIBN radical initiator (1 wt% relative to the combined weight of the monomers) in tetrahydrofuran and acetonitrile (2 : 1; v/v) solvent system at 60 °C for 2 days. All of these hybrid materials were characterized by using standard analytical and spectroscopic techniques including FT-IR, NMR, DLS, TEM and EDX.

FT-IR spectra of hybrids HA, HM and HMM were in good agreement with the proposed structures (see Fig. 1(A)–(C)). The vibrational bands observed for hybrids HA & HM in the range 1551–1573 cm^{-1} and 1416–1455 cm^{-1} correspond to the asymmetric and symmetric vibrations of deprotonated C–O group present in the acetate and methacrylate groups respectively. The vibrational bands observed in the range 668–421 cm^{-1} correspond to the stretching vibrations of HfO_2 particles.[27] The HMM hybrid polymer exhibited IR bands at 1755 and 1254 cm^{-1} due to C=O and CF_3 stretching respectively; whereas the bands observed in the range 1420–1578 cm^{-1} and 428–637 cm^{-1} correspond to the vibrations of the aromatic ring and HfO_2 particles respectively.[26,27]

Furthermore, the presence of various organic units in hybrids HA & HM and hybrid polymer HMM were confirmed by NMR analyses. The absence of carboxylic proton peaks in hybrids HA & HM suggests that the organic ligands in these hybrids are deprotonated (see ESI Fig. S2 and S4†). The proton resonance peaks appearing at 1.8–2.0 ppm for HA & HM are due to the methyl (–CH_3) groups of the organic units, as shown in Scheme 1. The peaks due to the methylene (=CH_2) protons of HM were located at 5.3–6.1 ppm. NMR data therefore confirm the attachment of organic ligands, methyl acetate and methyl methacrylate, on HfO_2 surface in hybrids HA & HM respectively as expected. The olefinic proton peaks of HM and MAPDST

Published on 07 July 2016. Downloaded by Indian Institute of Technology Mandi on 6/18/2020 12:12:14 PM.

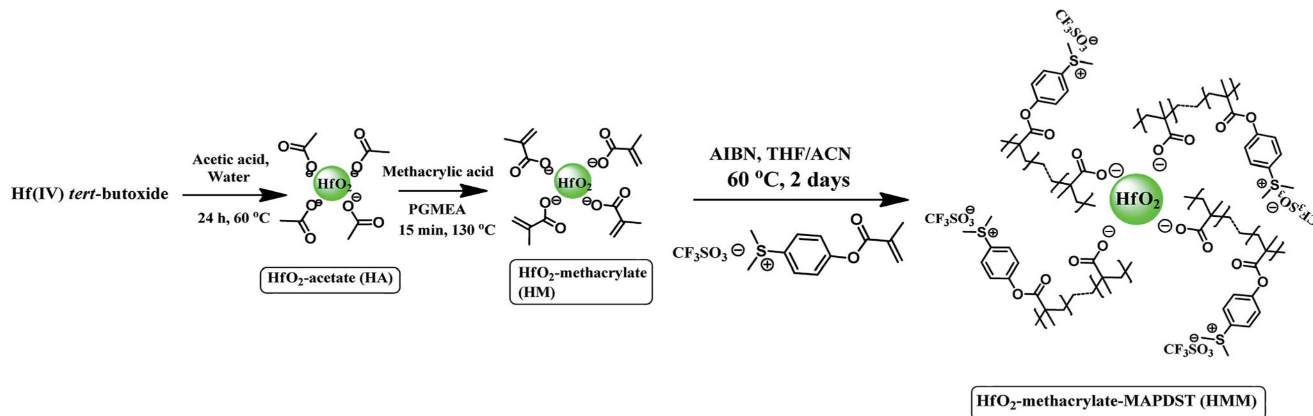

Scheme 1 Synthetic route of HMM hybrid polymer.

monomers were absent in the spectrum of HMM (see Fig. 1(D)) suggesting the complete conversion of monomers into polymer. For HMM hybrid polymer, the resonance peaks observed at 3.2 ppm can be assigned to the methyl protons on the sulfonium moiety, whereas, the aromatic protons of the phenyl rings appeared in the range 7.5–8.5 ppm. In addition, the appearance of broad peaks at 2.0–2.4 and 1.1–1.6 ppm due to the methylene and methyl protons respectively of the polymer skeleton (see Fig. 1(D)) indicate the formation of HMM hybrid polymer as expected. ^{19}F NMR analysis of HMM showed a peak at −77.64 ppm corresponding to $CF_3SO_3^-$ unit of MAPDST moiety.[17] The ^{13}C NMR signals observed at ppm values 178.26, 172.61 and 174.5 for HA, HM and HMM respectively indicate the presence of C═O group in their organic skeleton. In addition, HMM showed ^{13}C resonance signals at 29 and 45.5 ppm corresponding to $-SCH_3$ and polymeric $-CH_2-$ moieties respectively[21,26] (see ESI Fig. S3, S5 and S7† for more details).

The weight average molecular weight (M_w) of the hybrid polymer HMM was determined by gel permeation chromatography (GPC) using mixed-C column. 1% LiBr in DMF was used as the eluent for GPC analysis at a flow rate of 1 mL min^{-1} at 70 °C. Polyethylene oxide (PEO) and poly(ethyleneglycol) (PEG) standards were used for plotting the size exclusion chromatography (SEC) calibration curve. The average molecular weight (M_w) of HMM hybrid polymer was calculated to be 27 885 g mol^{-1} with a polydispersity index of 2.150 (see ESI Fig. S9†). EDX analyses were performed to confirm the presence of HfO_2 nano-particles in HMM, see ESI Fig. S10.† Thermogravimetric analyses (TGA) were conducted to investigate thermal stabilities of the hybrids. The decomposition temperature of HMM corresponding to 5% weight loss was 220 °C, indicating its sufficient thermal stability for lithographic applications, see ESI Fig. S11.†

The size and morphology of hybrids HA, HM and HMM were evaluated by using TEM and DLS studies. The TEM analysis

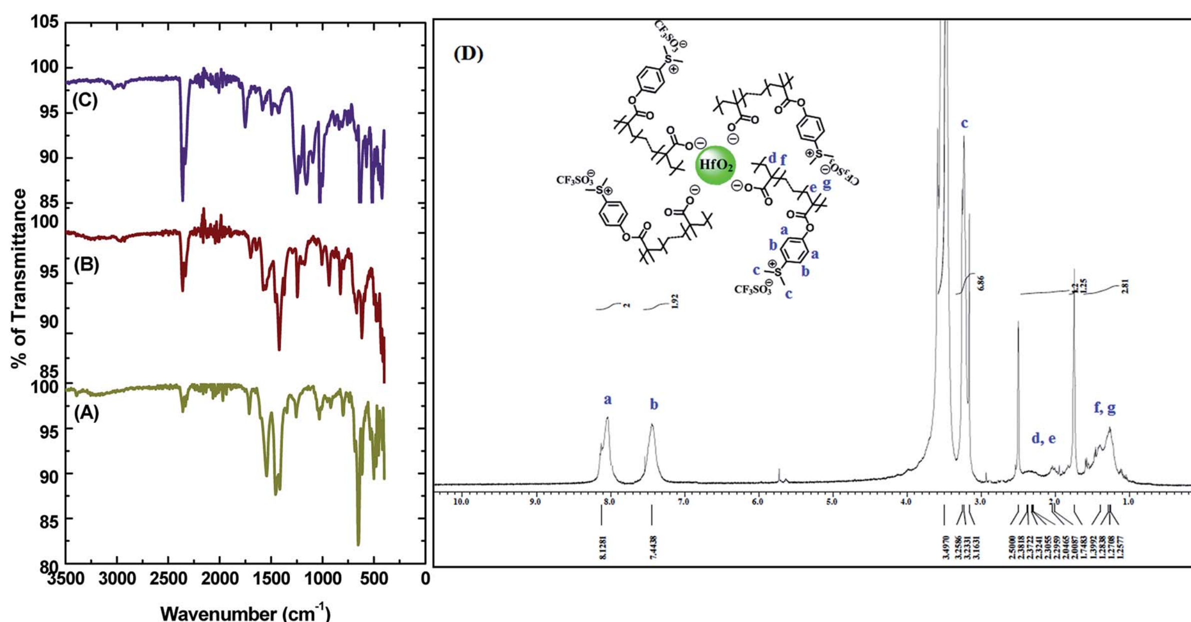

Fig. 1 FT-IR spectrum of hybrids HA (A), HM (B) and HMM (C) and ^{1}H NMR of HMM (D).

 This journal is © The Royal Society of Chemistry 2016

Published on 07 July 2016. Downloaded by Indian Institute of Technology Mandi on 6/18/2020 12:12:14 PM.

revealed that the hybrids HA & HM show almost similar sizes within the range 3–5 nm as expected (see ESI Fig. S12(A) and (B)†). The well-defined crystalline HfO_2 lattice structure of HM is shown in ESI Fig. S12(C).† The TEM analysis revealed a particle size of ~12 nm for HMM hybrid polymer, see ESI Fig. S12(D) and (E).† The significant increase in particle size of HMM compared to that of hybrids HA & HM could be attributed to the presence of large organic polymeric moiety around HfO_2 in HMM.[27] Furthermore, well-defined X-ray diffraction pattern of the HfO_2 particles of HMM is shown in Fig. S12(F), ESI.† The DLS studies revealed the hydrodynamic radii of hybrids HA, HM and HMM in acetonitrile solutions as 1–5 nm, 2–3 nm and 9–15 nm respectively; which are in agreement with the data obtained from TEM studies, see ESI Fig. S12(G).†

EUVL exposure

Evaluation of hybrid polymer HMM towards non-chemically amplified resist (n-CAR) application was realized with the exposure to extreme ultra-violet (EUV) radiation (λ = ~13.5 nm) through 0.3-NA optics of a Micro-field Exposure Tool (MET) at SEMATECH Berkeley, see ESI Fig. S13† for more details. Thin films of HMM having thickness of ~53 nm were used for EUV exposure studies. An E_0 center dose value of 22 mJ cm^{-2} was used for these exposures, which was lower than that used for pure MAPDST homopolymer resist (30 mJ cm^{-2}).[22] This indicated that the sensitivity of HMM hybrid resist is higher than that of the corresponding neat organic homopolymer resist probably due to the incorporation of HfO_2 nanoparticles in resist formulation. The results of EUV exposure studies are presented in Fig. 2. The high resolution features presented here contains the matrix of 5 : 1 duty cycle, space/line patterns printed with the feature sizes (printed@wafer) of 80 to 30 nm. Our efforts to get high resolution images of patterns with 1 : 1 duty cycle were unsuccessful and hence the resolution data reported here is based on 5 : 1 duty cycle patterns.

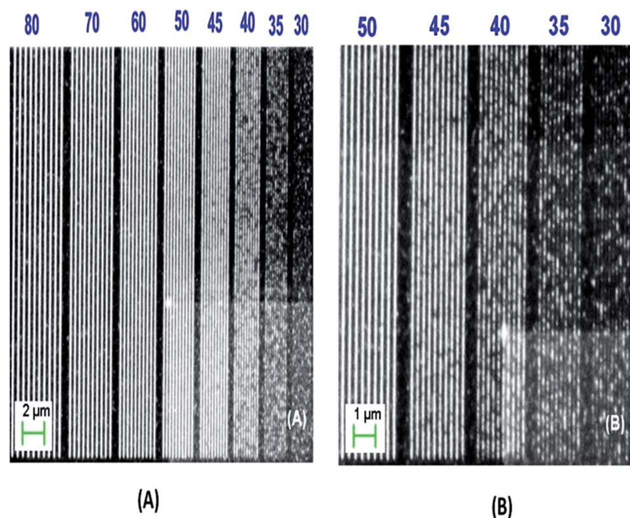

Fig. 2 FE-SEM images of EUV exposed HMM hybrid polymer resist for 5 : 1 duty cycle line patterns: (A) 80, 70, 60, 50, 45, 40, 35 and 30 nm at 10 KX (Mag) and (B) 50, 45, 40, 35, 30 nm at 25 KX (Mag).

It has been reported earlier that the particle sizes of certain Hf-based hybrid photoresists show a dramatic increase after UV exposure. The particle coarsening sensitivities of those hybrid resist nanoparticles were also consistent with their EUV performances.[16] Although the effects of UV on particle sizes of HMM resist were not explored in this study, it is worthwhile to note that the AFM images of HMM resist before and after EUV irradiation did not show any increase in surface roughness, even at the edges of the patterns. This perhaps points to a negligible variation in HMM hybrid particle size under the experimental conditions employed.

As can be seen in Fig. 2(A), 80 to 50 nm isolated line patterns of 5 : 1 duty cycle were very well resolved, but there were instigations of bridging observed for 45 nm line patterns and beyond, see Fig. 2(B). At higher resolutions, undesirable traits like pattern-collapse, fracturing, peel-off and de-adhesion were revealed. Bridging and fracturing were predominant for 35 and 30 nm patterns whereas peel-off and de-adhesion were common at even higher resolutions (not shown here).

AFM studies for modulus measurements

A clear understanding of the factors leading to the progressive variations in undesirable traits like bridging, fracturing, peel-off, de-adhesion and pattern-collapse exhibited by high resolution line patterns of HMM resist may help in designing improved hybrid photo resists for sub-20 nm applications. Therefore, a nano-mechanical, non-destructive analyses of the developed 5 : 1 duty cycle 80, 70, 40, 35, 30 nm line patterns of HMM resist were performed through Peak Force QNM-AFM analysis. Fig. 3(A)–(C) show the topography, modulus and adhesion of 80 & 70 nm isolated line patterns of HMM resist measured by Peak Force QNM tapping mode AFM. The computed root mean square (r.m.s) roughness for 80 & 70 nm line patterns shown in Fig. 3(A) was 14.2 nm; while the calculated DMT modulus and adhesion were 3.23 ± 0.2, 3.14 ± 0.15 GPa and 62 ± 5, 57 ± 3 nN respectively for these line patterns. Similarly, Fig. 3(D)–(F) show the topography, modulus and adhesion of 40, 35 & 30 nm line patterns of HMM resist respectively. The measured r.m.s roughness of line patterns shown in Fig. 3(D) was 9.86 nm and the calculated modulus and adhesion for 40, 35 & 30 nm line patterns mapped in Fig. 3(D)–(F) were 3.1 ± 0.19, 2.81 ± 0.18 & 2.65 ± 0.11 Gpa and 56 ± 3, 50 ± 2 & 50 ± 4 nN respectively. As shown in Fig. 3 (B) and (E), the magnitude of the calculated DMT modulus of HMM hybrid decreased ~18% with increase in line-pattern resolution from 80 to 30 nm for 5 : 1 duty cycles. This significant reduction in the magnitude of DMT modulus for higher resolution line patterns perhaps causes their undesirable traits such as bridging, fracturing, de-adhesion and peel-off.[3,4,24,25] Moreover, this effect will be more prominent during the development processes of EUV exposed resist films where capillary forces play a dominant role; especially in the case of high resolution isolated line patterns and densely featured patterns.[24,25] Similarly, as shown in Fig. 3(C) and (F), the adhesion magnitude decreased ~19% with increase in line pattern resolution from 80 to 30 nm for 5 : 1 duty cycles, which explains the observed fracturing, peel-off and collapsing of the printed high

Published on 07 July 2016. Downloaded by Indian Institute of Technology Mandi on 6/18/2020 12:12:14 PM.

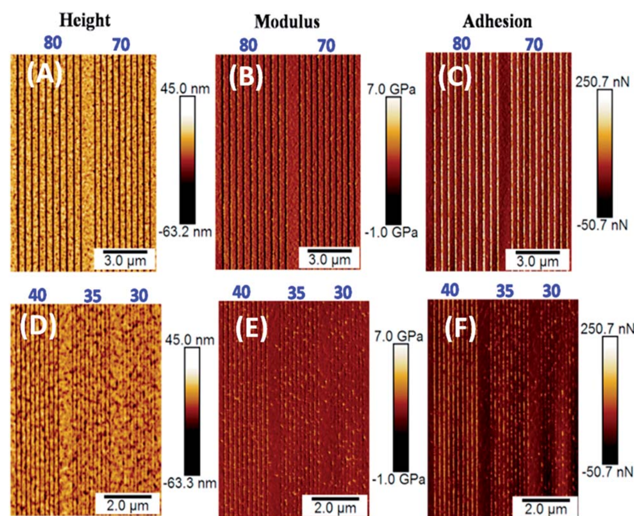

Fig. 3 Representative mapping of topography, DMT modulus and adhesion for EUV exposed HMM hybrid n-CAR resist for 5 : 1 duty cycle line patterns: (A), (B) and (C) show 80 & 70 nm line patterns; (D), (E) and (F) show 40, 35 & 30 nm line patterns.

resolution line patterns. For 35 nm and 30 nm line patterns, it was observed that the DMT modulus decreased when the resolution changed from 35 nm to 30 nm, while the adhesion value remained same. We believe that the lateral contribution of wafer Si towards adhesion plays an important role here. Fig. 3(C) clearly shows that the Si present between resist lines shows very high adhesion map. For 30 nm lines, severe pattern collapse was observed and therefore the measured adhesion value might get affected by the increased contact of AFM tip with the wafer Si during the scans resulting in higher adhesion value than expected.

Conclusions

We have developed a new hybrid resist formulation based on HfO_2–methacrylate and (methacryloyloxy)phenyl dimethyl sulfoniumtriflate and investigated its performance as a non-chemically amplified photoresist for high resolution EUVL pattering. EUVL results suggested that this new resist formulation is highly competent for pattering well resolved features of ~40 nm and above. However, below ~40 nm, line patterns exhibited undesirable traits like bridging, peel-off, de-adhesion and pattern collapse. Nano-mechanical property evaluations performed on EUV line patterns using Peak Force-Quantitative Nano-Mechanical (PF-QNM) tapping mode AFM analyses revealed a significant reduction in the modulus and adhesion magnitudes for higher resolution line patterns, which probably account for the undesirable traits exhibited by the resist at higher resolutions.

Acknowledgements

Acknowledgment is made to Intel Corp, USA, for partial support of the project administered by SRC USA. The authors would like to thank Dr Patrick Naulleau and Dr Chris Anderson (LBNL) for extreme ultraviolet exposure using Microfield Exposure Tool at LBNL. Acknowledgments are also due to Prof. Patricia Santiago, UNAM, Mexico for high resolution TEM images and Prof. Nikola Batina, Universidad Autónoma Metropolitana – Iztapalapa, Mexico for fruitful discussions on Peak Force QNM imaging analysis. AMRC, IIT Mandi is acknowledged for infrastructural facilities.

Notes and references

1 T. Itani and T. Kozawa, *Jpn. J. Appl. Phys.*, 2013, **52**, 010002–010014.
2 B. Wu and A. Kumar, *Appl. Phys. Res.*, 2014, **1**, 011101–011115.
3 J. Paul, M. Rudolph, S. Riedel, X. Thrun, S. Wege and C. Hohle, *Proc. SPIE*, 2013, **8685**, 86850V.
4 S. Kang, W. L. Wu, K. W. Choi, A. DeSilva, C. K. Ober and V. M. Prabhu, *Macromolecules*, 2010, **43**, 4275–4286.
5 M. Trikeriotis, M. Krysak, Y. S. Chung, C. Ouyang, B. Cardineau, R. Brainard, C. K. Ober, E. P. Giannelis and K. Cho, *J. Photopolym. Sci. Technol.*, 2012, **25**, 583–586.
6 H. Gokan, S. Esho and Y. Ohnishi, *J. Electrochem. Soc.*, 1983, **130**, 143–146.
7 K. E. Gonsalves, J. Wang and H. J. Wu, *J. Vac. Sci. Technol., B: Microelectron. Nanometer Struct.–Process., Meas., Phenom.*, 2000, **18**, 325–327.
8 H. W. Ro, V. Popova, L. Chen, A. M. Forster, Y. F. Ding, K. J. Alvine, D. J. Krug, R. M. Laine and C. L. Soles, *Adv. Mater.*, 2011, **23**, 414–420.
9 M. Krysak, M. Trikeriotis, E. Schwartz, N. Lafferty, P. Xie, B. Smith, P. Zimmerman, W. Montgomery, E. Giannelis and C. K. Ober, *Proc. SPIE*, 2011, **7972**, 79721C.
10 M. Trikeriotis, W. J. Bae, E. Schwartz, M. Krysak, N. Lafferty, P. Xie, B. Smith, P. A. Zimmerman, C. K. Ober and E. P. Giannelis, *Proc. SPIE*, 2010, **7639**, 76390E.
11 B. Cardineau, R. D. Re, M. Marnell, H. Al-Mashat, M. Vockenhuber, Y. Ekinci, C. Sarma, D. A. Freedman and R. L. Brainard, *Microelectron. Eng.*, 2014, **127**, 44–50.
12 J. Passarelli, B. Cardineau, R. D. Re, M. Sortland, M. Vockenhuber, Y. Ekinci, C. Sarma, M. Neisser, D. A. Freedman and R. L. Brainard, *Proc. SPIE*, 2014, **9051**, 90512A.
13 J. Passarelli, M. Sortland, R. D. Re, B. Cardineau, C. Sarma, D. A. Freedman and R. L. Brainard, *J. Photopolym. Sci. Technol.*, 2014, **27**, 655–661.
14 M. Kryask, M. Trikeriotis, C. Ouyang, S. Chakrabarty, E. P. Giannelis and C. K. Ober, *J. Photopolym. Sci. Technol.*, 2013, **26**, 659–664.
15 J. Jiang, B. Zhang, M. Yu, L. Li, M. Neisser, J. S. Chun, E. P. Giannelis and C. K. Ober, *J. Photopolym. Sci. Technol.*, 2015, **28**, 515–518.
16 L. Li, S. Chakrabarty, K. Spyrou, C. K. Ober and E. P. Giannelis, *Chem. Mater.*, 2015, **27**, 5027–5031.
17 V. Kalyani, V. S. V. Satyanarayana, V. Singh, C. P. Pradeep, S. Ghosh, S. K. Sharma and K. E. Gonsalves, *Chem.–Eur. J.*, 2015, **21**, 2250–2258.

This journal is © The Royal Society of Chemistry 2016

18 M. Krysak, M. Trikeriotis, E. Schwartz, N. Lafferty, P. Xie, B. Smith, P. Zimmerman, W. Montgomery, E. Giannelis and C. K. Ober, *Proc. SPIE*, 2011, **7972**, 79721C.
19 J. Jiang, S. Chakrabarty, M. Yu and C. K. Ober, *J. Photopolym. Sci. Technol.*, 2014, **27**, 663–666.
20 I. B. Baek, J. H. Yang, W. J. Cho, C. G. Ahn, K. Im and S. Lee, *J. Vac. Sci. Technol., B: Microelectron. Nanometer Struct.–Process., Meas., Phenom.*, 2005, **23**, 3120–3123.
21 V. Singh, V. S. V. Satyanarayana, S. K. Sharma, S. Ghosh and K. E. Gonsalves, *J. Mater. Chem. C*, 2014, **2**, 2118–2122.
22 V. S. V. Satyanarayana, F. Kessler, V. Singh, F. R. Scheffer, D. E. Weibel, S. Ghosh and K. E. Gonsalves, *ACS Appl. Mater. Interfaces*, 2014, **6**, 4223–4232.
23 G. R. Chagas, V. S. V. Satyanarayana, F. Kessler, G. K. Belmonte, K. E. Gonsalves and D. E. Weibel, *ACS Appl. Mater. Interfaces*, 2015, **7**, 16348–16356.
24 P. K. Kulshreshtha, K. Maruyama, S. Kiani, D. Ziegler, J. Blackwell, D. Olynick and P. D. Ashby, *Proc. SPIE*, 2013, **8681**, 868100.
25 G. Winroth, R. Gronheid, T. G. Kim and P. W. Mertens, *Microelectron. Eng.*, 2012, **98**, 159–162.
26 V. S. V. Satyanarayana, V. Singh, V. Kalyani, C. P. Pradeep, S. Sharma, S. Ghosh and K. E. Gonsalves, *RSC Adv.*, 2014, **4**, 59817–59820.
27 W. J. Bae, M. Trikeriotis, J. Sha, E. L. Schwartz, R. Rodriguez, P. Zimmerman, E. P. Giannelis and C. K. Ober, *J. Mater. Chem.*, 2010, **20**, 5186–5189.

Published on 07 July 2016. Downloaded by Indian Institute of Technology Mandi on 6/18/2020 12:12:14 PM.